Quantitative Methods in Finance Final Project: Barrier Option Pricing Models

Benjamin Cartwright and Azfina Anindita

December 2025

Abstract

This project studies the pricing of European vanilla and down-and-out barrier call options using analytical, simulation-based, and numerical partial differential equation methods. Closed-form Black–Scholes formulas and Monte Carlo simulation of geometric Brownian motion are used as baseline models for vanilla options, and these methods are extended and compared for down-and-out barrier options. Additional pricing approaches include a finite-difference Crank–Nicolson solution of the Black–Scholes PDE and Monte Carlo simulation under the Heston stochastic volatility model. Five structured computational experiments analyze baseline consistency, sensitivity to barrier level, volatility scaling, and maturity, as well as Monte Carlo convergence behavior. The results demonstrate theoretical price ordering, strong agreement among Black–Scholes– based methods, and systematic differences introduced by stochastic volatility and path dependence.

1 Introduction

This project investigates the pricing of European vanilla call options and European down-and-out barrier call options using a combination of analytical, simulation-based, and numerical partial differential equation methods. The primary objective is to compare model behavior, numerical accuracy, and convergence properties across pricing approaches under both constant-volatility and stochastic-volatility assumptions. A sequence of five structured computational experiments is used to analyze baseline pricing consistency, sensitivity to barrier level, volatility scaling, maturity, and Monte Carlo sample size.

A European vanilla call option gives the holder the right, but not the obligation, to purchase an asset at strike price K at maturity T. Its payoff depends only on the terminal asset price S_T and is given by

$$(S_T - K)^+,$$

making vanilla options path independent. Under the Black–Scholes framework, vanilla call options admit an exact closed-form solution and can also be priced using Monte Carlo simulation of geometric Brownian motion.

A European down-and-out barrier call option has the same terminal payoff structure but is extinguished if the underlying asset price falls below a fixed barrier level $B < S_0$ at any time prior to maturity. Its payoff can be written as

$$(S_T - K)^+ \cdot \mathbf{1}_{\{\min_{0 \le t \le T} S_t > B\}},$$

introducing strong path dependence. Because the option may be knocked out before maturity, barrier options are strictly cheaper than their vanilla counterparts with otherwise identical parameters.

Under the risk-neutral measure, the Black–Scholes model assumes the asset price follows a geometric Brownian motion

$$dS_t = S_t(r - q)\,dt + \sigma S_t\,dW_t,$$

where r is the risk-free rate, q is a continuous dividend yield, and σ is the volatility. This dynamics leads to the Black–Scholes partial differential equation for the option value $V(S, t)$, with barrier options differing from vanilla options only through their boundary conditions, such as the absorbing condition $V(B, t) = 0$ for down-and-out options.

While closed-form pricing formulas exist for both vanilla and certain barrier options under the Black–Scholes model, numerical methods are essential for validating results, studying convergence, and extending pricing to more complex settings. In this project, vanilla options are priced using closed-form Black–Scholes formulas and Monte Carlo simulation as baseline references. These same methods are applied to down-and-out barrier options alongside finite-difference solutions of the Black–Scholes PDE and Monte Carlo simulation under the Heston stochastic volatility model. The five experiments collectively assess how barrier risk, volatility, maturity, and numerical resolution affect option prices and model agreement.

2 Theory

This section provides a mathematical representation of vanilla European call options and European down and out barrier call options. It then reviews the theoretical framework of the options pricing models used throughout this project.

2.1 European Vanilla Options

A European call option gives the holder the right, but not the obligation, to purchase an asset at strike price K at maturity T. The payoff is:

$$\text{Payoff} = (S_T - K)^+,$$

where S_T is the underlying asset price at maturity.

Vanilla options are *not path-dependent*: only the terminal price matters. This makes them amenable to closed-form solutions under the Black–Scholes model and straightforward Monte Carlo pricing.

2.2 European Down-and-Out Barrier Options

A down-and-out call option has the same payoff at maturity, but only if the price has remained strictly above a barrier B throughout the contract:

$$\text{Payoff} = (S_T - K)^+ \cdot \mathbf{1}_{\{\min_{0\le t\le T} S_t > B\}}.$$

This option is *path-dependent*. If the asset ever hits the barrier level $B < S_0$, the option is knocked out and becomes worthless. Because of this path dependence, additional tools such as the reflection principle and Brownian Bridge corrections are needed for accurate pricing.

2.3 The Black–Scholes Model

Under the risk-neutral measure Q, the asset price evolves according to a Geometric Brownian Motion (GBM):

$$dS_t = S_t(r - q)\,dt + \sigma S_t\,dW_t,$$

where:

- r is the risk-free rate,
- q is a continuous dividend yield,
- σ is volatility,
- W_t is a standard Brownian motion.

The SDE has closed-form solution:

$$S_T = S_0 \exp\left[(r - q - (1/2)\sigma^2)T + \sigma W_T\right].$$

2.3.1 Black–Scholes PDE

Let $V(S, t)$ denote the option price at time t when the asset price is S. The Black–Scholes PDE is:

$$\frac{\partial V}{\partial t} + (1/2)\sigma^2 S^2 \frac{\partial^2 V}{\partial S^2} + (r - q)S\frac{\partial V}{\partial S} - rV = 0.$$

For a European call, the terminal condition is:

$$V(S, T) = (S_T - K)^+.$$

Barrier options modify this PDE via boundary conditions, e.g. for a down-and-out option:

$$V(B, t) = 0 \quad \text{for all } t < T.$$

2.4 Closed-Form Black–Scholes Pricing for Vanilla Options

Define:

$$d_1 = \frac{\ln\left(\frac{S_0}{K}\right) + (r - q + (1/2)\sigma^2)T}{\sigma\sqrt{T}}, \qquad d_2 = d_1 - \sigma\sqrt{T}.$$

Let $N(\cdot)$ denote the CDF of the standard normal distribution. Then the Black–Scholes price of a European call is:

$$C_{\mathrm{BS}} = S_0 e^{-qT} N(d_1) - K e^{-rT} N(d_2).$$

This price is exact, deterministic, and extremely fast to compute.

2.5 Monte Carlo Pricing of Vanilla Options

Using the GBM solution, one simulates M independent paths:

$$S_T^{(i)} = S_0 \exp\left[(r - q - (1/2)\sigma^2)T + \sigma\sqrt{T}Z_i\right], \quad Z_i \sim N(0,1).$$

The Monte Carlo estimator for a call is:

$$\hat{C}_{\mathrm{MC}} = e^{-rT}\,\frac{1}{M}\sum_{i=1}^{M}(S_T^{(i)} - K)^+.$$

This converges to the Black–Scholes price as $M \to \infty$.

2.6 Closed-Form Black–Scholes Pricing for Down-and-Out Options

Barrier options satisfy the same PDE as vanilla options but with an *absorbing boundary* at $S = B$. The solution uses the *method of images*, based on the reflection principle for Brownian motion. The idea is that any path that crosses the barrier can be reflected across the barrier to form a "mirror image" path, which corresponds to subtracting a term from the vanilla price.

Let:

$$\lambda = \frac{r - q}{\sigma^2} - \frac{1}{2}.$$

Then the closed-form down-and-out call price is:

$$C_{\mathrm{DOC}} = C_{\mathrm{BS}}(S_0) - \left(\frac{B}{S_0}\right)^{2\lambda - 2} C_{\mathrm{BS}}\left(\frac{B^2}{S_0}\right),$$

where $C_{\mathrm{BS}}(\cdot)$ is the standard Black–Scholes call formula. The second term removes the contribution of all paths that hit the barrier.

2.7 Monte Carlo Pricing of Down-and-Out Options

A naive Monte Carlo simulation checks whether the simulated discrete path ever crosses the barrier. However, GBM evolves in continuous time, and barrier crossings may occur between the simulated discrete time points. This leads to a positive bias: some paths that should be knocked out are mistakenly kept.

2.7.1 Discrete Monitoring Problem

When you simulate a GBM path with time steps Δt:

$$S_{t+\Delta t} = S_t \exp\left[(r - q - \frac{1}{2}\sigma^2)\Delta t \, + \, \sigma\sqrt{\Delta t}\, Z\right],$$

you only know the asset price at the discrete grid points:

$$t_0 = 0, \quad t_1 = \Delta t, \quad t_2 = 2\Delta t, \quad \ldots, \quad t_N = T.$$

Even if both endpoints of a time interval satisfy $S_{t_k} > B$ and $S_{t_{k+1}} > B$, the continuous-time price path may still have touched the barrier B at some intermediate time. Standard Monte Carlo simulation fails to detect such barrier hits.

2.7.2 Brownian Bridge Correction

To fix this, we use a Brownian Bridge between the two simulated points. Let $X_t = \ln S_t$ and $b = \ln B$. Conditioned on X_{t_k} and $X_{t_{k+1}}$, the process inside the interval behaves like a Brownian Bridge with known first-passage probabilities.

The probability of hitting the barrier inside the interval $[t_k, t_{k+1}]$ is:

$$p_{\text{hit},k} = \exp\left(-\frac{2(X_{t_k} - b)\,(X_{t_{k+1}} - b)}{\sigma^2(t_{k+1} - t_k)}\right).$$

The probability that the barrier is *not* hit in the interval is $1 - p_{\text{hit},k}$. Over the entire path:

$$p_{\text{survive}} = \prod_{k=0}^{N-1} (1 - p_{\text{hit},k}).$$

The Monte Carlo payoff becomes:

$$\text{Payoff}^{(i)} = e^{-rT}\,(S_T^{(i)} - K)^+ \, p_{\text{survive}},$$

providing a smoothed estimator that correctly accounts for continuous barrier monitoring while using a discrete simulation grid.

2.8 Finite-Difference Pricing via the Crank–Nicolson Method

Finite-difference methods provide a deterministic numerical approach to option pricing by solving the Black–Scholes partial differential equation directly on a discretized grid in asset price and time. In this project, we use the Crank–Nicolson (CN) scheme, which is second-order accurate in both space and time and unconditionally stable.

2.8.1 Vanilla European Call Options

For vanilla European call options, the Black–Scholes PDE

$$\frac{\partial V}{\partial t} + \frac{1}{2}\sigma^2 S^2 \frac{\partial^2 V}{\partial S^2} + (r-q)S\frac{\partial V}{\partial S} - rV = 0$$

is solved on a truncated spatial domain

$$S \in [0, S_{\max}],$$

where $S_{\max}$ is chosen sufficiently large so that the asymptotic behavior of the option is well captured.

Boundary conditions are imposed to match the limiting behavior of a call option:

$$V(0,t) = 0, \qquad V(S_{\max}, t) \approx S_{\max} e^{-q(T-t)} - K e^{-r(T-t)}.$$

The terminal condition at maturity is given by the standard European call payoff:

$$V(S,T) = (S-K)^+.$$

The PDE is discretized in space using central finite differences and in time using a uniform backward grid. The Crank–Nicolson scheme averages the spatial differential operator between successive time levels, yielding a linear system of the form

$$(I - A)V^n = (I + A)V^{n+1},$$

where A represents the discretized Black–Scholes operator. Due to the local nature of the finite-difference stencil, this system is tridiagonal and can be solved efficiently at each time step using the Thomas algorithm. The solution is marched backward from maturity to the present, and the option price is obtained by interpolating the grid solution at $S = S_0$. As the grid is refined, the finite-difference price converges to the closed-form Black–Scholes solution.

2.8.2 Down-and-Out European Call Barrier Options

For down-and-out European call options, the same Black–Scholes PDE is solved, but the presence of a barrier introduces path dependence through boundary conditions. The spatial domain is shifted to

$$S \in [B, S_{\max}],$$

where B is the barrier level.

The barrier is enforced via an absorbing boundary condition:

$$V(B,t) = 0 \quad \text{for all } t < T,$$

which ensures that the option is immediately knocked out upon barrier breach. This condition is imposed explicitly at every time step to prevent numerical drift.

The terminal condition remains

$$V(S,T) = (S-K)^+ \quad \text{for } S \geq B,$$

with the barrier node forced to zero. At the upper boundary, the same asymptotic call condition is applied:

$$V(S_{\max}, t) \approx S_{\max} e^{-q(T-t)} - K e^{-r(T-t)}.$$

The Crank–Nicolson discretization proceeds as in the vanilla case, but only interior grid points are solved at each time step, with boundary values incorporated into the right-hand side of the linear system. The resulting tridiagonal system is solved using the Thomas algorithm, and the solution is marched backward in time. The option price at inception is obtained by interpolating the numerical solution at $S = S_0$, with the understanding that if $S_0 \leq B$ the option value is zero.

This finite-difference formulation provides a direct PDE-based representation of barrier option pricing under Black–Scholes and serves as a deterministic benchmark for comparison with Monte Carlo and closed-form barrier pricing methods.

2.9 Monte Carlo Pricing under the Heston Stochastic Volatility Model

To study the impact of stochastic volatility on barrier option pricing, this project implements Monte Carlo pricing under the Heston model. Unlike the Black–Scholes framework, where volatility is constant, the Heston model allows the instantaneous variance to evolve randomly over time, capturing volatility clustering and leverage effects commonly observed in equity markets.

2.9.1 The Heston Model

Under the risk-neutral measure Q, the Heston model assumes the joint dynamics

$$\frac{dS_t}{S_t} = (r-q)\,dt + \sqrt{v_t}\,dW_t^S,$$

$$dv_t = \kappa(\theta - v_t)\,dt + \xi\sqrt{v_t}\,dW_t^v,$$

with correlated Brownian motions satisfying

$$dW_t^S\,dW_t^v = \rho\,dt.$$

Here, v_t denotes the instantaneous variance, κ controls the speed of mean reversion toward the long-run variance θ, ξ is the volatility of variance, and ρ governs the correlation between asset returns and variance shocks. The initial variance is v_0.

2.9.2 Monte Carlo Discretization

The coupled system is simulated using an Euler-type time discretization with step size $\Delta t = T/N$. Correlated Brownian increments are constructed as

$$\Delta W_t^v = \sqrt{\Delta t}\, Z_2, \qquad \Delta W_t^S = \sqrt{\Delta t}\,\big(\rho Z_2 + \sqrt{1-\rho^2}\, Z_1\big),$$

where $Z_1, Z_2 \sim \mathcal{N}(0,1)$ are independent standard normal variables.

The variance process is advanced via

$$v_{t+\Delta t} = v_t + \kappa(\theta - v_t)\Delta t + \xi\sqrt{v_t}\,\Delta W_t^v,$$

and the asset price is updated using a log-Euler scheme,

$$S_{t+\Delta t} = S_t \exp\!\left((r - q - \frac{1}{2}v_t)\Delta t + \sqrt{v_t}\,\Delta W_t^S\right).$$

To maintain nonnegativity of the variance process, a *full truncation* scheme is used: negative variance values are clipped to zero when computing both drift and diffusion terms, and the updated variance is projected back to R_+ at each step. Antithetic variates are optionally employed to reduce estimator variance.

2.9.3 Down-and-Out Barrier Implementation

The down-and-out European call option payoff under Heston dynamics is

$$(S_T - K)^+ \cdot \mathbf{1}_{\{\min_{0\le t\le T} S_t > B\}}.$$

Barrier enforcement is handled in two complementary ways. First, if a simulated path crosses the barrier at a discrete time point, the option is immediately knocked out and its payoff is set to zero. Second, to account for possible barrier crossings between discrete monitoring times, a local Brownian-bridge-style correction is applied.

Let $X_t = \log S_t$ and $b = \log B$. Conditioned on X_{t_k} and $X_{t_{k+1}}$, the log price increment over a small interval is approximated as Gaussian with variance given by the integrated variance over the step. This integral is approximated locally by

$$\int_{t_k}^{t_{k+1}} v_s\, ds \;\approx\; \bar{v}\,\Delta t, \qquad \bar{v} = \frac{1}{2}\big(v_{t_k} + v_{t_{k+1}}\big).$$

The probability of hitting the barrier within the interval is then approximated by

$$p_{\text{hit}} = \exp\!\left(-\frac{2(X_{t_k} - b)(X_{t_{k+1}} - b)}{\bar{v}\,\Delta t}\right),$$

and the survival probability over the entire path is obtained by multiplying the complements of these probabilities across all time steps.

The discounted Monte Carlo estimator is given by

$$\hat{C}_{\text{Heston}} = e^{-rT}\,\frac{1}{M}\sum_{i=1}^{M}(S_T^{(i)} - K)^{+}\mathbf{1}_{\{\text{not knocked out}\}}\,p_{\text{survive}}^{(i)}.$$

This approach provides a practical approximation to continuously monitored barrier options under stochastic volatility and enables direct comparison with Black–Scholes barrier prices and finite-difference solutions.

3 Experiments and Expectations

This section summarizes the numerical experiments conducted in this project and the theoretical expectations guiding their interpretation. The experiments compare pricing methods for European vanilla call options and European down-and-out call barrier options under constant- and stochastic-volatility assumptions.

Unless otherwise stated, all experiments use identical contract specifications (S_0, K, r, q) and pricing implementations across the same set of equities. Throughout all experiments, vanilla options are priced using both the closed-form Black–Scholes formula and Monte Carlo simulation of GBM paths.

3.1 Experiments, Expectations, and Interpretation

Baseline Model Comparison This experiment compares all pricing methods for vanilla and down-and-out barrier options. We vary the barrier level, stock ticker and volatility scale. Our goal is to establish baseline agreement across analytical, simulation-based, and numerical PDE approaches.

Expectation. Constant-volatility Black–Scholes methods should agree up to numerical and sampling error, vanilla options should dominate barrier options, and stochastic volatility under the Heston model should further reduce barrier prices:

$$C_{\text{DO}}^{\text{Heston}} \;\le\; C_{\text{DO}}^{\text{MC}} \;\approx\; C_{\text{DO}}^{\text{BS}} \;\approx\; C_{\text{DO}}^{\text{FD}} \;<\; C_{\text{vanilla}}^{\text{BS}} \;\approx\; C_{\text{vanilla}}^{\text{MC}}.$$

Barrier Level Sweep This experiment varies the down-and-out barrier level to isolate the effect of barrier proximity relative to the spot price, using vanilla options as a reference.

Expectation. As the barrier increases toward S_0, the probability of knock-out decreases and barrier option prices increase monotonically, while vanilla prices remain invariant:

$$\frac{\partial C_{\text{DO}}}{\partial B} > 0, \qquad \frac{\partial C_{\text{vanilla}}}{\partial B} = 0.$$

Volatility Scaling Sweep This experiment examines how changes in volatility affect vanilla and barrier option prices, emphasizing the interaction between volatility and barrier risk.

Expectation. Vanilla call prices increase monotonically with volatility, while barrier option prices increase more slowly due to elevated knock-out probability:

$$\frac{\partial C_{\mathrm{DO}}}{\partial \sigma} < \frac{\partial C_{\mathrm{vanilla}}}{\partial \sigma}.$$

Time-to-Maturity Sweep This experiment studies how option prices evolve with maturity for both vanilla and barrier options.

Expectation. Vanilla call prices increase with maturity, whereas barrier option prices grow more slowly as longer horizons increase cumulative barrier breach probability:

$$\frac{\partial C_{\mathrm{vanilla}}}{\partial T} > 0,$$

while down-and-out barrier option prices exhibit weaker time sensitivity due to the declining probability of barrier survival, implying

$$\frac{\partial C_{\mathrm{DO}}}{\partial T} < \frac{\partial C_{\mathrm{vanilla}}}{\partial T}.$$

Moreover, for a nontrivial down barrier $B < S_0$, the price gap between vanilla and barrier options typically widens with maturity:

$$C_{\mathrm{vanilla}}(T) - C_{\mathrm{DO}}(T) \text{ is nondecreasing in } T.$$

Monte Carlo Convergence This experiment evaluates the convergence of Monte Carlo estimators by increasing the number of simulated paths and comparing results to analytical benchmarks.

Expectation. Monte Carlo estimators converge to their analytical Black–Scholes prices at rate $\mathcal{O}(M^{-1})$, with slower convergence for barrier options due to path dependence and barrier detection.

4 Results

4.1 Experiment 1: Baseline Model Comparison

	Ticker	Barrier_frac	vol_scale	MC_GBM_Vanilla	BS_Vanilla	MC_GBM_DownOut	BS_DownOut_Images	FD_CN_DownOut	Heston_MC_DownOut
0	AAPL	0.85	0.8	8.411808	8.391133	8.408618	8.391124	8.391091	8.185965
1	AAPL	0.85	1.0	10.344297	10.317659	10.338977	10.316905	10.316875	10.121431
2	AAPL	0.85	1.2	12.277663	12.244580	12.262938	12.235117	12.235068	12.023664
3	AAPL	0.90	0.8	8.411808	8.391133	8.400414	8.382535	8.383293	8.126029
4	AAPL	0.90	1.0	10.344297	10.317659	10.269078	10.244097	10.244580	9.943107
5	AAPL	0.90	1.2	12.277663	12.244580	12.006927	11.975347	11.975629	11.621220
6	AAPL	0.95	0.8	8.411808	8.391133	7.740977	7.713985	7.714178	7.257673
7	AAPL	0.95	1.0	10.344297	10.317659	8.801443	8.763095	8.763134	8.334939
8	AAPL	0.95	1.2	12.277663	12.244580	9.592563	9.544453	9.544438	9.154618
9	AMZN	0.85	0.8	8.438172	8.416466	8.433908	8.415893	8.415869	8.255746
10	AMZN	0.85	1.0	10.408984	10.380657	10.392690	10.368882	10.368836	10.191069
11	AMZN	0.85	1.2	12.379990	12.344411	12.307024	12.274321	12.274241	12.058223
12	AMZN	0.90	0.8	8.438172	8.416466	8.378933	8.358448	8.358848	8.112903
13	AMZN	0.90	1.0	10.408984	10.380657	10.133489	10.105691	10.105895	9.807599
14	AMZN	0.90	1.2	12.379990	12.344411	11.658291	11.621430	11.621524	11.285917
15	AMZN	0.95	0.8	8.438172	8.416466	7.193313	7.162429	7.162463	6.810853
16	AMZN	0.95	1.0	10.408984	10.380657	7.982600	7.938594	7.938578	7.628977
17	AMZN	0.95	1.2	12.379990	12.344411	8.528741	8.492963	8.492935	8.218311
18	JPM	0.85	0.8	8.794928	8.773739	8.791792	8.773738	8.773694	8.522580
19	JPM	0.85	1.0	10.795346	10.768219	10.790965	10.768098	10.768064	10.539085
20	JPM	0.85	1.2	12.797069	12.763564	12.788538	12.761007	12.760967	12.530998
21	JPM	0.90	0.8	8.794928	8.773739	8.789208	8.771261	8.772290	8.481611
22	JPM	0.90	1.0	10.795346	10.768219	10.760402	10.736282	10.737000	10.419340
23	JPM	0.90	1.2	12.797069	12.763564	12.647956	12.616797	12.617259	12.244973
24	JPM	0.95	0.8	8.794928	8.773739	8.319796	8.298588	8.298967	7.764835
25	JPM	0.95	1.0	10.795346	10.768219	9.591488	9.549951	9.550067	9.034822
26	JPM	0.95	1.2	12.797069	12.763564	10.558434	10.507598	10.507613	10.027676

Figure 1: Experiment 1: Baseline Option Prices Across Models.

4.2 Experiment 2: Barrier Level Sweep

In this experiment, we study how down-and-out call option prices depend on the barrier level and how numerical methods compare to the Black–Scholes benchmark. We define the *knock-out penalty* as

$$\text{Penalty} \;\equiv\; C_{\text{vanilla}} - C_{\text{down-and-out}},$$

which measures the loss in option value induced by the presence of the barrier.

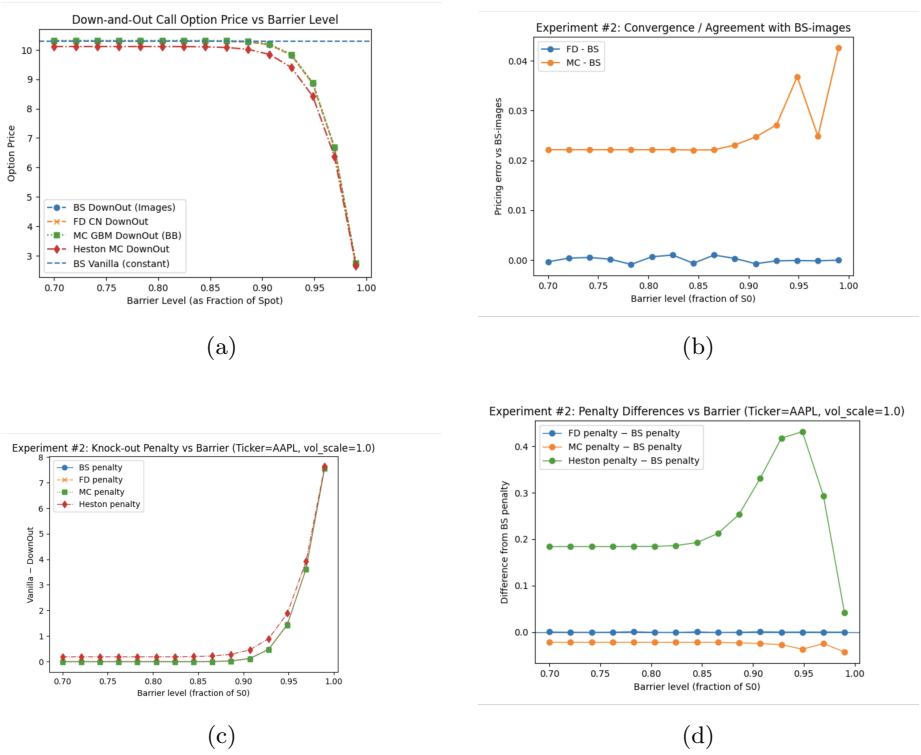

Figure 2: Experiment 2: Barrier Level Sweep Results

(a) **Down-and-out price vs barrier level.** This figure shows that down-and-out call prices remain close to the vanilla option value when the barrier is far below the spot price, indicating negligible knock-out risk. As the barrier approaches the spot, prices collapse rapidly toward zero, reflecting the sharply increasing probability of early termination. All constant-volatility methods agree closely across the entire barrier range, while the stochastic volatility model consistently produces lower prices, especially near high barriers, due to increased downside risk.

(b) **Agreement with the Black–Scholes images solution.** This figure illustrates the pricing error of numerical methods relative to the Black–Scholes images benchmark. The finite difference method exhibits errors that are effectively zero across all barrier levels, indicating strong numerical convergence. Monte Carlo errors are larger and grow near high barriers, reflecting increased variance and sensitivity to barrier crossings rather than systematic bias.

(c) **Knock-out penalty vs barrier level.** This plot shows the knock-out penalty—the value lost relative to a vanilla option—as a function of the barrier level. The penalty is negligible for low barriers and increases

sharply as the barrier approaches the spot price, highlighting the nonlinear sensitivity of barrier options. Constant-volatility methods produce nearly identical penalties, while the stochastic volatility model yields a significantly larger penalty, indicating a higher likelihood of knock-out events.

(d) **Penalty differences relative to Black–Scholes.** This figure isolates deviations from the Black–Scholes knock-out penalty. The finite difference penalty is indistinguishable from the benchmark, confirming numerical accuracy. Monte Carlo penalties are slightly lower, reflecting residual sampling error. In contrast, the stochastic volatility penalty is substantially higher across most barrier levels, demonstrating genuine model-driven differences rather than numerical artifacts.

4.3 Experiment 3: Volatility Scaling Sweep

In this experiment, we examine how down-and-out call option prices and knock-out penalties respond to changes in volatility, with the barrier fixed at $B = 0.85S_0$. Volatility is scaled as

$$\sigma = \alpha\, \sigma_{\text{hist}},$$

where α is a multiplicative volatility factor. The following figures summarize the results across four complementary views.

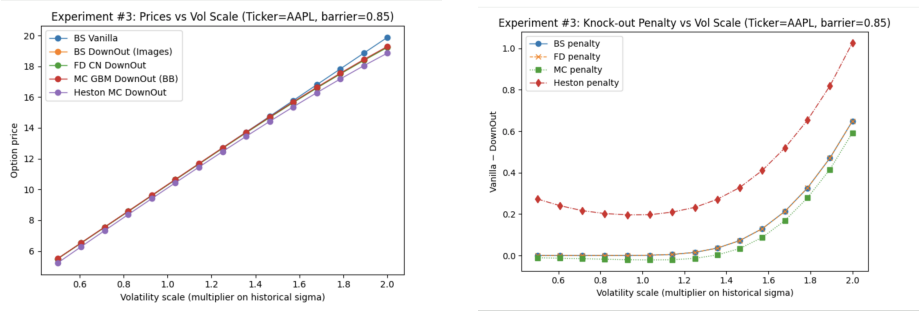

(a) (b)

Figure 3: Experiment 3: Volatility Scaling Sweep Results

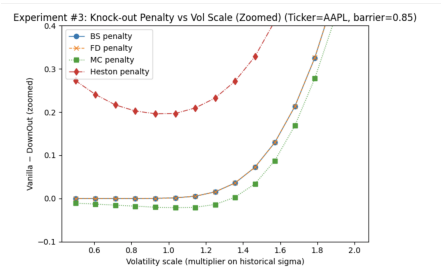

(c)

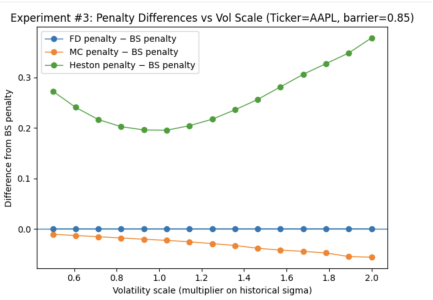

(d)

Figure 3: Experiment 3: Volatility Scaling Sweep Results (continued)

(a) **Option prices vs volatility scale.** This figure shows that option prices increase monotonically with volatility due to increased upside optionality. However, down-and-out option prices grow more slowly than the vanilla price, reflecting the offsetting effect of higher knock-out probability at larger volatility levels. All constant-volatility methods produce nearly identical prices, while the stochastic volatility model yields consistently lower values, with the gap widening as volatility increases.

(b) **Knock-out penalty vs volatility scale.** This plot shows how the knock-out penalty increases with volatility. The penalty is small at low volatility, indicating that the barrier rarely binds, but rises rapidly as volatility increases. Constant-volatility methods agree closely across the entire range, while the stochastic volatility model produces a substantially larger penalty, reflecting increased downside risk under stochastic variance dynamics.

(c) **Knock-out penalty vs volatility (zoomed).** This zoomed view highlights the low-to-moderate volatility regime, where the penalty begins to emerge from zero. The nonlinear onset of the penalty is evident, demonstrating that even moderate increases in volatility can materially increase knock-out risk. Differences between constant-volatility models remain negligible, while the stochastic volatility penalty is already significantly elevated.

(d) **Penalty differences relative to Black–Scholes.** This figure isolates deviations of the knock-out penalty from the Black–Scholes benchmark. Finite difference penalties are effectively indistinguishable from the benchmark, confirming numerical convergence. Monte Carlo penalties exhibit a small negative bias that grows with volatility. In contrast, the stochastic volatility penalty is consistently and substantially higher, demonstrating genuine model-driven differences rather than numerical error.

Overall, Experiment 3 shows that volatility is a primary driver of barrier risk: while higher volatility increases option value, it simultaneously amplifies

knock-out probability. Constant-volatility models remain mutually consistent across all volatility levels, whereas stochastic volatility introduces materially higher penalties, particularly in high-volatility regimes.

4.4 Experiment 4: Time-to-Maturity Sweep

In this experiment, we study how down-and-out call option prices and knock-out penalties vary with time to maturity, holding the barrier fixed at $B = 0.85S_0$ and volatility fixed at its historical level.

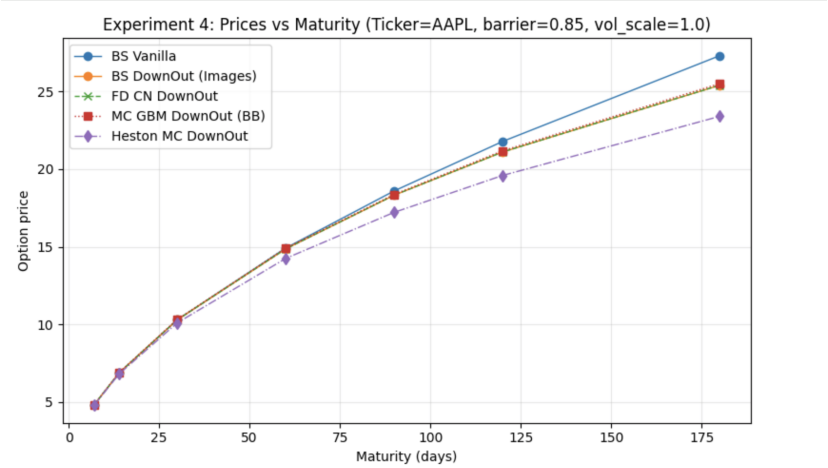

Figure 4: Experiment 4: Maturity Sweep Results (Figure 1)

Option prices vs maturity. This figure shows that option prices increase monotonically with maturity, reflecting the growing value of time optionality. For short maturities, all models produce nearly identical prices, indicating that the barrier has limited impact when there is little time for the underlying to reach it. As maturity increases, the gap between vanilla and down-and-out prices widens, reflecting increased knock-out risk over longer horizons. Constant-volatility methods remain tightly clustered across all maturities, while the stochastic volatility model produces consistently lower prices, with the discrepancy growing as maturity increases.

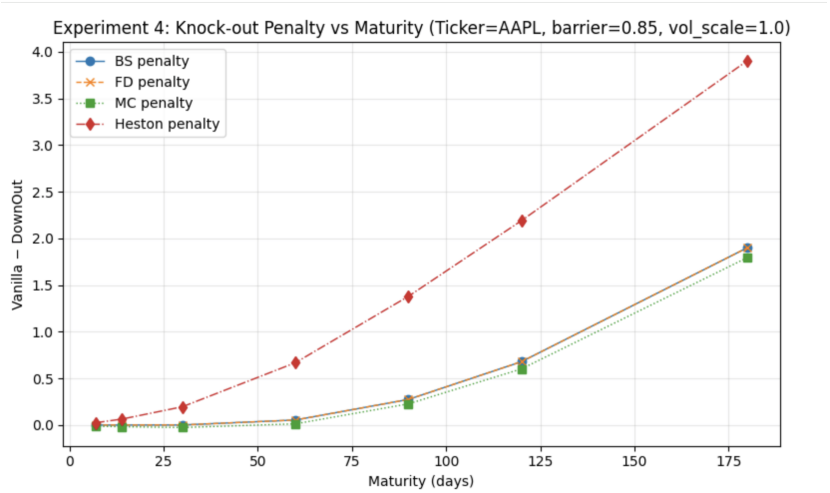

Figure 5: Experiment 4: Maturity Sweep Results (Figure 2)

Knock-out penalty vs maturity. This plot shows how the knock-out penalty increases with time to maturity. The penalty is negligible at short maturities, indicating minimal probability of barrier breach, but grows rapidly as maturity increases, reflecting cumulative knock-out risk over time. Constant-volatility models yield nearly identical penalties, while the stochastic volatility model produces a substantially larger penalty at all maturities, highlighting the amplified downside risk induced by stochastic variance dynamics.

Overall, Experiment 4 demonstrates that maturity is a key driver of barrier risk: longer-dated options face significantly higher knock-out penalties despite higher overall option values. While constant-volatility models remain consistent across maturities, stochastic volatility introduces materially larger penalties, particularly for long-dated options.

4.5 Experiment 5: Monte Carlo Convergence

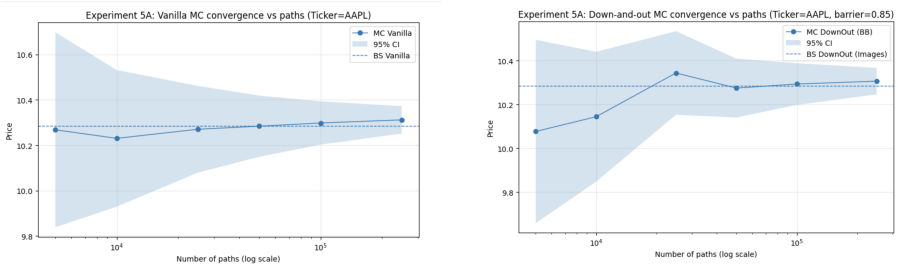

(a) Caption for E5_1

(b) Caption for E5_2

Figure 6: Experiment 5: Monte Carlo Convergence (Part 1)

(a) **Vanilla option Monte Carlo convergence.** This figure shows Monte Carlo estimates of the vanilla call option price as a function of the number of simulated paths. As the number of paths increases, the Monte Carlo estimate stabilizes and converges toward the Black–Scholes benchmark. The confidence intervals shrink steadily with increasing path count, illustrating the reduction in sampling uncertainty. The estimates remain centered around the benchmark, indicating an absence of systematic bias.

(b) **Down-and-out option Monte Carlo convergence.** This figure shows the same convergence behavior for the down-and-out call option. While the Monte Carlo estimates again converge toward the benchmark price, the convergence is slower and the confidence intervals are wider at low path counts, reflecting the increased variance introduced by barrier monitoring. As the number of paths increases, uncertainty diminishes and the estimates stabilize near the benchmark value.

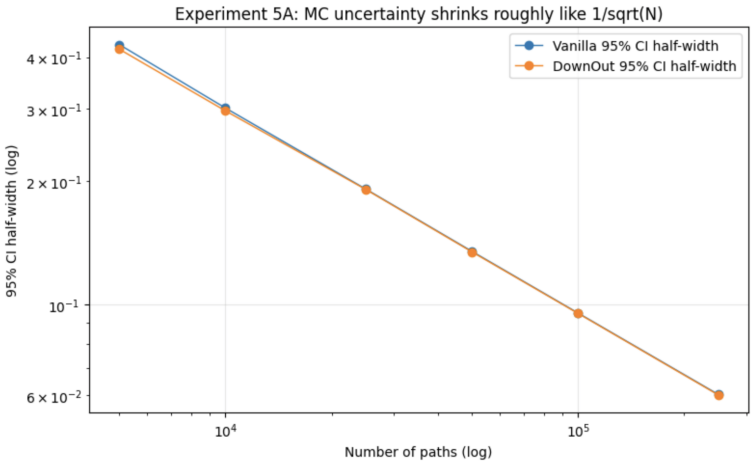

Figure 7: Experiment 5: Monte Carlo Convergence (Part 2)

- **Monte Carlo uncertainty vs number of paths.** This figure demonstrates that Monte Carlo uncertainty decreases approximately at the theoretical rate of $\mathcal{O}(1/\sqrt{N})$, where N is the number of simulated paths. On the log–log scale, the confidence interval half-widths for both vanilla and down-and-out options follow nearly linear trends with similar slopes, indicating consistent convergence behavior. The close alignment of the two curves shows that, despite higher variance at low path counts for barrier options, both option types ultimately exhibit the same asymptotic convergence rate.

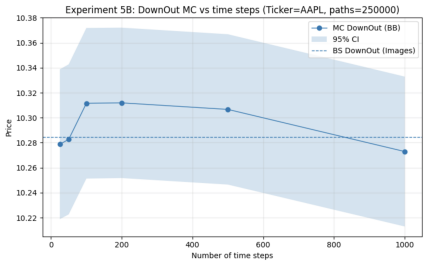

(a) Caption for E5_4

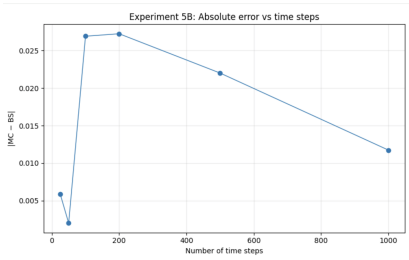

(b) Caption for E5_5

Figure 8: Experiment 5: Monte Carlo Convergence (Part 3)

(a) **Down-and-out Monte Carlo price vs time steps.** This figure shows the Monte Carlo estimate of the down-and-out call option price as a function of the number of time steps. At coarse discretizations, the estimate

exhibits noticeable bias due to missed barrier crossings. As the number of time steps increases, the estimate stabilizes and approaches the benchmark value. Beyond a moderate number of time steps, further refinement yields diminishing returns, indicating that discretization error becomes small relative to Monte Carlo sampling error.

(b) **Absolute pricing error vs time steps.** This figure quantifies the absolute deviation of the Monte Carlo estimate from the benchmark price as a function of time-step resolution. The error decreases as the number of time steps increases, confirming convergence of the time-discretized Monte Carlo scheme. The non-monotonic behavior at very low step counts reflects competing effects of discretization bias and sampling noise, while the overall downward trend demonstrates improved accuracy with finer temporal resolution.

5 Analysis

Overall, the results align closely with the expectations stated in Section 3. Vanilla prices from Monte Carlo and closed-form Black–Scholes agree up to sampling error, confirming baseline consistency when both methods price the same constant-volatility GBM model. Across all experiments, down-and-out options remain strictly cheaper than their vanilla counterparts, as expected from the knock-out feature.

Experiments 2–4 confirm the main comparative statics of barrier options. As the barrier approaches spot, down-and-out prices collapse and the knock-out penalty

$$\text{Penalty} \equiv C_{\text{vanilla}} - C_{\text{down-and-out}}$$

increases sharply, while vanilla prices remain effectively barrier-invariant. Increasing volatility raises both vanilla and barrier prices, but the barrier price rises more slowly because higher volatility also increases barrier breach probability, producing a larger penalty. Increasing maturity raises option values overall, but the barrier penalty grows with maturity due to accumulating knock-out risk over a longer horizon.

Within the Black–Scholes constant-volatility setting, the numerical methods exhibit the expected agreement: the images solution, Crank–Nicolson finite differences, and Monte Carlo with Brownian-bridge correction remain tightly clustered, with differences consistent with discretization and sampling error. Deviations are most visible near high barriers or extreme settings where barrier survival becomes rare and Monte Carlo variance increases.

The main systematic contrast comes from stochastic volatility. Heston Monte Carlo prices for down-and-out options are consistently lower (and penalties larger) than the Black–Scholes-based barrier prices, matching the expectation that stochastic variance and downside volatility dynamics increase the likelihood of barrier breach relative to a constant-volatility model.

Finally, Experiment 5 confirms Monte Carlo convergence properties: confidence intervals shrink with increasing path count in a manner consistent with $\mathcal{O}(1/\sqrt{N})$, and improving time-step resolution reduces barrier-monitoring discretization error. Together, these findings support the reliability of the implementations and reinforce the theoretical behavior of barrier option pricing across barrier level, volatility, and maturity.

6 Justification of Expectations

6.1 Experiment 1

Under the Black–Scholes model, the asset price S_t follows geometric Brownian motion with constant volatility σ:

$$dS_t = rS_t\,dt + \sigma S_t\,dW_t,$$

where r is the risk-free interest rate and W_t is a standard Brownian motion under the risk-neutral measure Q.

All Black–Scholes–based pricing methods compute the same discounted risk-neutral expectation of the option payoff:

$$C = e^{-rT}\,E^Q[\text{payoff}(S)].$$

Hence, up to discretization and sampling error,

$$C_{\text{DO}}^{\text{MC}} \;\approx\; C_{\text{DO}}^{\text{BS}} \;\approx\; C_{\text{DO}}^{\text{FD}}, \qquad C_{\text{vanilla}}^{\text{MC}} \;\approx\; C_{\text{vanilla}}^{\text{BS}}.$$

The payoff of a European vanilla call option is

$$(S_T - K)^+,$$

where S_T is the asset price at maturity T and K is the strike price.

The payoff of a European down-and-out call option with barrier $B < S_0$ is

$$\mathbf{1}_{\{\tau_B > T\}}(S_T - K)^+,$$

where $\mathbf{1}_{\{\cdot\}}$ denotes the indicator function and

$$\tau_B = \inf\{t \le T : S_t \le B\}$$

is the first time the asset price hits the barrier.

For every price path,

$$\mathbf{1}_{\{\tau_B > T\}}(S_T - K)^+ \le (S_T - K)^+,$$

with strict inequality on a set of positive probability whenever $P(\tau_B \le T) > 0$. Taking discounted expectations yields

$$C_{\text{DO}} < C_{\text{vanilla}}.$$

Under the Heston stochastic volatility model, the asset price S_t and instantaneous variance v_t satisfy

$$dS_t = rS_t\,dt + \sqrt{v_t}\,S_t\,dW_t^S,$$
$$dv_t = \kappa(\theta - v_t)\,dt + \xi\sqrt{v_t}\,dW_t^v,$$

where v_t is the instantaneous variance, $\kappa > 0$ is the mean-reversion speed, $\theta > 0$ is the long-run variance, and $\xi > 0$ is the volatility of variance.

The Brownian motions W_t^S and W_t^v satisfy

$$\operatorname{corr}(dW_t^S, dW_t^v) = \rho < 0.$$

Negative return–volatility correlation implies that downward shocks to the asset price tend to coincide with upward shocks to variance:

$$S_t \downarrow \Rightarrow\ v_t \uparrow .$$

Higher instantaneous variance increases the probability of large short-term price fluctuations. In particular, for any fixed barrier $B < S_t$, higher variance raises the probability that the price process crosses the barrier before maturity:

$$v_t \uparrow \Rightarrow\ P(\tau_B \le T \mid \mathcal{F}_t) \uparrow .$$

Combining these effects yields

$$S_t \downarrow \Rightarrow\ v_t \uparrow \Rightarrow\ P(\tau_B \le T) \uparrow .$$

The down-and-out call payoff

$$\mathbf{1}_{\{\tau_B > T\}}(S_T - K)^+$$

is highly sensitive to barrier survival. Under Heston dynamics with $\rho < 0$, downward price movements both move the asset closer to the barrier and increase volatility, which further raises the likelihood of barrier breach.

As a result, the survival indicator $\mathbf{1}_{\{\tau_B > T\}}$ is stochastically smaller under Heston dynamics than under constant-volatility Black–Scholes calibrated to an average volatility level. Consequently,

$$E^Q\big[\mathbf{1}_{\{\tau_B > T\}}(S_T - K)^+\big]_{\text{Heston}} \ \le\ E^Q\big[\mathbf{1}_{\{\tau_B > T\}}(S_T - K)^+\big]_{\text{BS}}\,.$$

Discounting preserves the ordering, implying

$$C_{\text{DO}}^{\text{Heston}} \le C_{\text{DO}}^{\text{BS}}.$$

This inequality is not a pathwise identity but an expectation-level ordering that holds generically for equity-style Heston calibrations, particularly when $\rho < 0$ and the barrier is nontrivially close to the spot price.

Combining model equivalence under constant volatility, payoff dominance of barrier options, and stochastic volatility effects under equity-style Heston dynamics yields the expected ordering

$$C_{\text{DO}}^{\text{Heston}} \ \le\ C_{\text{DO}}^{\text{MC}} \ \approx\ C_{\text{DO}}^{\text{BS}} \ \approx\ C_{\text{DO}}^{\text{FD}} \ <\ C_{\text{vanilla}}^{\text{BS}} \ \approx\ C_{\text{vanilla}}^{\text{MC}}.$$

6.2 Experiment 2

Let S_t be a continuous price process with initial value $S_0 > B$, and define the first hitting time of a down barrier B by

$$\tau_B := \inf\{t \in [0,T] : S_t \le B\}.$$

The down-and-out call payoff is

$$\Pi_B := \mathbf{1}_{\{\tau_B > T\}}(S_T - K)^+.$$

Pathwise monotonicity in the barrier. Let $B_1 < B_2 < S_0$. Then, by definition of the hitting time,

$$\{\tau_{B_2} > T\} \subseteq \{\tau_{B_1} > T\}.$$

Equivalently,

$$\mathbf{1}_{\{\tau_{B_2} > T\}} \le \mathbf{1}_{\{\tau_{B_1} > T\}} \quad \text{a.s.}$$

Multiplying by the nonnegative payoff $(S_T - K)^+$ yields the pathwise ordering

$$\mathbf{1}_{\{\tau_{B_2} > T\}}(S_T - K)^+ \;\le\; \mathbf{1}_{\{\tau_{B_1} > T\}}(S_T - K)^+.$$

Expectation-level ordering. Taking discounted risk-neutral expectations preserves the inequality:

$$C_{\mathrm{DO}}(B_2) = e^{-rT}\,E^Q\Big[\mathbf{1}_{\{\tau_{B_2} > T\}}(S_T - K)^+\Big] \;\le\; e^{-rT}\,E^Q\Big[\mathbf{1}_{\{\tau_{B_1} > T\}}(S_T - K)^+\Big] = C_{\mathrm{DO}}(B_1).$$

Thus,

$$B_1 < B_2 \quad \Longrightarrow \quad C_{\mathrm{DO}}(B_2) \le C_{\mathrm{DO}}(B_1),$$

with strict inequality whenever $P(\tau_{B_2} \le T) > 0$.

Differential form. If the mapping $B \mapsto C_{\mathrm{DO}}(B)$ is differentiable, the monotonicity implies

$$\frac{\partial C_{\mathrm{DO}}}{\partial B} < 0, \qquad B \in (0, S_0).$$

Interpretation. Raising a down barrier enlarges the knock-out set:

$$B \uparrow \Longrightarrow\; \{\tau_B \le T\} \uparrow \Longrightarrow\; \mathbf{1}_{\{\tau_B > T\}} \downarrow \Longrightarrow\; C_{\mathrm{DO}}(B) \downarrow .$$

6.3 Experiment 3

Let $\sigma \mapsto S_t^{(\sigma)}$ denote the asset price process with volatility σ, and define the down-and-out barrier hitting time

$$\tau_B^{(\sigma)} := \inf\{t \le T : S_t^{(\sigma)} \le B\}.$$

The vanilla and down-and-out call prices are given by

$$C_{\mathrm{vanilla}}(\sigma) = e^{-rT}\,E^Q\Big[(S_T^{(\sigma)} - K)^+\Big],$$

$$C_{\mathrm{DO}}(\sigma) = e^{-rT}\,E^Q\Big[\mathbf{1}_{\{\tau_B^{(\sigma)} > T\}}(S_T^{(\sigma)} - K)^+\Big].$$

Decomposition. Define the knock-out loss

$$L(\sigma) := (S_T^{(\sigma)} - K)^+ - \mathbf{1}_{\{\tau_B^{(\sigma)} > T\}}(S_T^{(\sigma)} - K)^+ = \mathbf{1}_{\{\tau_B^{(\sigma)} \le T\}}(S_T^{(\sigma)} - K)^+ \ge 0.$$

Then

$$C_{\mathrm{DO}}(\sigma) = C_{\mathrm{vanilla}}(\sigma) - e^{-rT}\, E^Q[L(\sigma)].$$

Volatility monotonicity. For a down barrier $B < S_0$,

$$\sigma_1 < \sigma_2 \quad \Longrightarrow \quad P\Big(\tau_B^{(\sigma_2)} \le T\Big) \ge P\Big(\tau_B^{(\sigma_1)} \le T\Big),$$

implying

$$\frac{\partial}{\partial \sigma} E^Q[L(\sigma)] > 0 \quad \text{(generically)}.$$

Sensitivity inequality. Differentiating the decomposition yields

$$\frac{\partial C_{\mathrm{DO}}}{\partial \sigma} = \frac{\partial C_{\mathrm{vanilla}}}{\partial \sigma} - e^{-rT} \frac{\partial}{\partial \sigma} E^Q[L(\sigma)],$$

and therefore

$$\frac{\partial C_{\mathrm{DO}}}{\partial \sigma} < \frac{\partial C_{\mathrm{vanilla}}}{\partial \sigma}.$$

Interpretation.

$$\sigma \uparrow \Longrightarrow\ P(\tau_B \le T) \uparrow \Longrightarrow\ E^Q[L(\sigma)] \uparrow \Longrightarrow\ \frac{\partial C_{\mathrm{DO}}}{\partial \sigma} < \frac{\partial C_{\mathrm{vanilla}}}{\partial \sigma}.$$

6.4 Experiment 4

Setup. Let S_t be a continuous risk-neutral price process with $S_0 > 0$, maturity $T > 0$, strike K, risk-free rate r, and down barrier $B < S_0$. Define the first barrier hitting time

$$\tau_B := \inf\{t \le T : S_t \le B\}.$$

The vanilla call price is

$$C_{\mathrm{vanilla}}(T) := e^{-rT}\, E^Q\left[(S_T - K)^+\right],$$

and the down-and-out call price is

$$C_{\mathrm{DO}}(T) := e^{-rT}\, E^Q\left[\mathbf{1}_{\{\tau_B > T\}}(S_T - K)^+\right].$$

Vanilla call monotonicity in maturity. For $0 < T_1 < T_2$, by the tower property,

$$C_{\text{vanilla}}(T_2) = e^{-rT_1}\, E^Q\Big[E^Q\Big(e^{-r(T_2-T_1)}(S_{T_2}-K)^+ \mid \mathcal{F}_{T_1}\Big)\Big].$$

Since $(x-K)^+$ is convex and the conditional distribution of $S_{T_2} \mid S_{T_1}$ has strictly larger dispersion for $T_2 > T_1$,

$$E^Q\Big(e^{-r(T_2-T_1)}(S_{T_2}-K)^+ \mid S_{T_1}\Big) \geq (S_{T_1}-K)^+,$$

with strict inequality under nondegenerate volatility. Hence

$$C_{\text{vanilla}}(T_2) > C_{\text{vanilla}}(T_1), \qquad \frac{\partial C_{\text{vanilla}}}{\partial T} > 0.$$

Barrier option decomposition. Define the knock-out loss

$$L(T) := (S_T-K)^+ - \mathbf{1}_{\{\tau_B > T\}}(S_T-K)^+ = \mathbf{1}_{\{\tau_B \leq T\}}(S_T-K)^+ \geq 0.$$

Then

$$C_{\text{DO}}(T) = C_{\text{vanilla}}(T) - e^{-rT}\, E^Q[L(T)].$$

Maturity effect on the knock-out penalty. For $T_1 < T_2$,

$$\{\tau_B \leq T_1\} \subseteq \{\tau_B \leq T_2\} \quad \Longrightarrow \quad \mathbf{1}_{\{\tau_B \leq T_1\}} \leq \mathbf{1}_{\{\tau_B \leq T_2\}}.$$

Thus $E^Q[L(T)]$ is nondecreasing in T, and generically strictly increasing for a nontrivial barrier.

Comparison of time sensitivities. Differentiating the decomposition yields

$$\frac{\partial C_{\text{DO}}}{\partial T} = \frac{\partial C_{\text{vanilla}}}{\partial T} - \frac{\partial}{\partial T}\Big(e^{-rT} E^Q[L(T)]\Big),$$

and since

$$\frac{\partial}{\partial T}\Big(e^{-rT} E^Q[L(T)]\Big) \geq 0,$$

it follows that

$$\frac{\partial C_{\text{DO}}}{\partial T} < \frac{\partial C_{\text{vanilla}}}{\partial T}.$$

Widening vanilla–barrier gap. From

$$C_{\text{vanilla}}(T) - C_{\text{DO}}(T) = e^{-rT}\, E^Q[L(T)],$$

and monotonicity of $E^Q[L(T)]$, the price gap

$$C_{\text{vanilla}}(T) - C_{\text{DO}}(T) \text{ is nondecreasing in } T.$$

6.5 Experiment 5

Let

$$X := e^{-rT}\,\Phi(S), \qquad C := E^{Q}[X],$$

where Φ denotes the payoff functional (vanilla or barrier). Given M i.i.d. samples $\{X_i\}_{i=1}^{M}$, define the Monte Carlo estimator

$$\widehat{C}_M := \frac{1}{M}\sum_{i=1}^{M} X_i.$$

By the Strong Law of Large Numbers,

$$\widehat{C}_M \to C \quad \text{a.s.}$$

and by the Central Limit Theorem,

$$\sqrt{M}\big(\widehat{C}_M - C\big) \to \mathcal{N}\big(0, \mathrm{Var}(X)\big),$$

in distribution. Implying

$$E\Big[(\widehat{C}_M - C)^2\Big] = \frac{\mathrm{Var}(X)}{M} = \mathcal{O}(M^{-1}).$$

For vanilla options,

$$X_{\text{vanilla}} = e^{-rT}(S_T - K)^+ \quad \Longrightarrow \quad \mathrm{Var}(X_{\text{vanilla}}) \text{ is moderate.}$$

For barrier options,

$$X_{\text{DO}} = e^{-rT}\mathbf{1}_{\{\tau_B > T\}}(S_T - K)^+,$$

which is path-dependent and discontinuous in the sample path, yielding

$$\mathrm{Var}(X_{\text{DO}}) > \mathrm{Var}(X_{\text{vanilla}}).$$

Hence, although both estimators satisfy

$$\widehat{C}_M - C = \mathcal{O}_p(M^{-1/2}),$$

the larger variance for barrier payoffs implies slower practical convergence for a given M, despite the same asymptotic rate.

7 References

References

[1] Black, F. and Scholes, M. (1973). The Pricing of Options and Corporate Liabilities. *Journal of Political Economy*, 81(3), 637–654.

[2] Hull, J. C. (2022). *Options, Futures, and Other Derivatives* (11th ed.). Pearson.

[3] Heston, S. L. (1993). A Closed-Form Solution for Options with Stochastic Volatility with Applications to Bond and Currency Options. *Review of Financial Studies*, 6(2), 327–343.

[4] Glasserman, P. (2003). *Monte Carlo Methods in Financial Engineering*. Springer.

[5] Tavella, D. and Randall, C. (2000). *Pricing Financial Instruments: The Finite Difference Method*. Wiley.

[6] Broadie, M., Glasserman, P., and Kou, S. (1997). A Continuity Correction for Discrete Barrier Options. *Mathematical Finance*, 7(4), 325–349.